Genetic Deletion of ABP-120 Alters the Three-dimensional Organization of Actin Filaments in *Dictyostelium* Pseudopods

Dianne Cox, J. Andrew Ridsdale, John Condeelis, and John Hartwig*

Department of Anatomy and Structural Biology, Albert Einstein College of Medicine, Bronx, New York 10461; and
*Experimental Medicine Division, Brigham & Women's Hospital, Harvard Medical School, Boston, Massachusetts 02115

Abstract. This study extends the observations on the defects in pseudopod formation of ABP-120$^+$ and ABP-120$^-$ cells by a detailed morphological and biochemical analysis of the actin based cytoskeleton. Both ABP-120$^+$ and ABP-120$^-$ cells polymerize the same amount of F-actin in response to stimulation with cAMP. However, unlike ABP-120$^+$ cells, ABP-120$^-$ cells do not incorporate actin into the Triton X-100–insoluble cytoskeleton at 30–50 s, the time when ABP-120 is incorporated into the cytoskeleton and when pseudopods are extended after cAMP stimulation in wild-type cells. By confocal and electron microscopy, pseudopods extended by ABP-120$^-$ cells are not as large or thick as those produced by ABP-120$^+$ cells and in the electron microscope, an altered filament network is found in pseudopods of ABP-120$^-$ cells when compared to pseudopods of ABP-120$^+$ cells. The actin filaments found in areas of pseudopods in ABP-120$^+$ cells either before or after stimulation were long, straight, and arranged into space filling orthogonal networks. Protrusions of ABP-120$^-$ cells are less three-dimensional, denser, and filled with multiple foci of aggregated filaments consistent with collapse of the filament network due to the absence of ABP-120–mediated cross-linking activity. The different organization of actin filaments may account for the diminished size of protrusions observed in living and fixed ABP- 120$^-$ cells compared to ABP-120$^+$ cells and is consistent with the role of ABP-120 in regulating pseudopod extension through its cross-linking of actin filaments.

PSEUDOPOD extension is an essential feature of many types of cell locomotion. Amoeboid cells in particular are well known for their reliance on pseudopod extension for locomotion. In chemotactic amoebae such as *Dictyostelium discoideum*, pseudopod extension appears to be a primary event in the reorganization of cytoskeletal polarity that is required for chemotaxis. Despite the demonstrated or suspected importance of the pseudopod in many cell types and after extensive study, modern cell biology has had difficulty in distinguishing definitively among the three general actin based models for how pseudopods are extended (Cooper, 1991; Egelhoff and Spudich, 1991; Condeelis, 1992; Fukui 1993; Lee et al., 1993; Oster and Perelson, 1995; Zigmond, 1993).

Part of the problem arises from the complexity of the actin cytoskeleton which contains a multitude of actin binding proteins potentially involved in the temporal and spatial control of actin polymerization, filament cross-linking, and sliding (Hartwig and Kwiatkowski, 1991; Luna and Hitt, 1992; Condeelis, 1993*a*). Taking advantage of model cell populations that exhibit protrusive activity and extend pseudopods synchronously in response to defined stimulation, such as platelets (Hartwig, 1992), neutrophils (Omann, 1987), and *Dictyostelium* (Condeelis, 1993*b*), a subset of actin binding proteins specifically involved in pseudopod extension have been tentatively identified. One of these proteins is ABP-120.

Immunofluorescence demonstrates that ABP-120 is concentrated in lamellipods and pseudopods during cell spreading and locomotion, and preferentially in pseudopods during cAMP-stimulated pseudopod extension (Condeelis 1981; Carboni and Condeelis, 1985; Condeelis et al., 1988). ABP-120 is incorporated into the actin cytoskeleton at times after stimulation with cAMP that correlate with cross-linking of actin into the cytoskeleton and pseudopod extension (Hall et al., 1988; Dharmawardhane et al., 1989). ABP-120 cross-links actin filaments in vitro to form a rigid actin gel containing orthogonal networks similar to those observed in pseudopods in situ (Condeelis et al., 1984, Wolosewick and Condeelis, 1986; Ogihara et al., 1988).

ABP-120 is a 40-nm rod-shaped protein consisting of two identical subunits each with a molecular mass of 120,000 D

The data in this paper are from a thesis to be submitted in partial fulfillment of the requirements for the Degree of Doctor of Philosophy in the Sue Golding Graduate Division of Medical Sciences, Albert Einstein College of Medicine, Yeshiva University.

Address all correspondence to Dianne Cox, Dept. of Anatomy and Structural Biology, Albert Einstein College of Medicine, 1300 Morris Park Ave., Bronx, NY 10461. Tel.: (718) 430-4113. FAX: (718) 518-7236.

on SDS-PAGE (Condeelis et al., 1984) or 92,200 D as inferred from sequence analysis (Noegel et al., 1989). Each monomer contains an amino-terminal actin filament-binding site which is highly conserved throughout a number of actin-binding protein families (Bresnick et al., 1990, 1991). The tail of each monomer contains six cross-beta sheet motifs that form the rod and probably function in dimer formation (Noegel et al., 1989; Bresnick et al., 1990). The subunits are packed in an anti-parallel orientation (Brink et al., 1990) consistent with its F-actin cross-linking activity.

The structural properties of ABP-120 suggest that it is a member of the ABP-280 family of actin-binding proteins. The tails of both ABP-120 and ABP-280 contain the repetitive beta-sheet motif and the amino-terminal actin-binding domains contain the conserved 27-amino acid actin-binding site (Gorlin et al., 1990). In addition, ABP-120 shares with macrophage ABP-280 the ability to promote orthogonal cross-links between actin filaments in vitro (Niederman et al., 1983; Wolosewick and Condeelis, 1986).

To evaluate the function of ABP-120 in vivo, we have used targeted gene disruption in two separate strains of *Dictyostelium*. In both strains, deletion of expression of ABP-120 results in mutants cells that are less active in pseudopod extension, exhibit a decrease in rate of formation and size of pseudopods, show reduced pseudopod extension activity after stimulation with a pulse of cAMP and have decreased efficiency of chemotaxis and rate of cell locomotion. In these mutants, the amount of F-actin that is incorporated into the cytoskeleton in response to stimulation with cAMP is significantly reduced (Cox et al., 1992). In a related study ABP-120$^-$ cells were produced by chemical mutagenesis. Although defects in motility were not reported, alterations in the incorporation of actin into the cytoskeleton were observed after stimulation of cells with cAMP (Brink et al., 1990). Both studies support a role for ABP-120 in regulating the organization of actin filaments in vivo. Furthermore, results from studies reporting defects in cell motility support a direct role for ABP-120–mediated filament cross-linking in normal pseudopod extension and cell locomotion (Cox et al., 1992).

In this study we report the first direct test of the hypothesis that ABP-120 is involved in filament cross-linking in vivo. The detailed morphological and biochemical analysis of the actin-based cytoskeleton of ABP-120$^+$ and ABP-120$^-$ cells reported here also allows direct correlation between the morphology and fine structure of the leading edge cytoskeleton of these cells with differences in motile behavior reported previously.

Materials and Methods

Cell Lines

ABP-120$^+$ and ABP-120$^-$ cell lines used were AX3-1S-2$^+$ and AX3-1S-4$^-$, respectively, and were derived from an AX3 parental *Dictyostelium* strain as described previously (Cox et al., 1992).

Antibodies

Affinity-purified rabbit anti-ABP-120 used throughout this study has been characterized to be monospecific to ABP-120 as described elsewhere (Carboni and Condeelis, 1985). The fluorescein-labeled goat anti-rabbit secondary antibody (Cappel; Organon Teknika, Rockville, MD) was preabsorbed against a fixed and permeabilized cell suspension as previously described (Condeelis et al., 1987) to remove antibodies that recognize *Dictyostelium* antigens.

NBD-Phallacidin Binding Assay

The NBD-phallacidin binding assay was performed as described in Hall et al. (1988) with minor modifications. The final fixation mixture contained 2×10^6 cells in 103 mM KPO_4, 10 mM PIPES, 18 mM KOH, 5 mM EGTA, 2 mM $MgSO_4$, 0.1% Triton X-100, 3.7% formaldehyde, and 0.4 mM caffeine in 1.5 ml final volume. The fixed cells were then stained with 0.4 μM NBD- phallacidin for 1 h and washed once with saponin buffer. The bound NBD-phallacidin was eluted from the cell pellet with 0.5 ml of absolute methanol for 30 min. The amount of NBD-phallacidin released was determined by the amount of emission of a sample at 465-nm excitation and 535-nm emission using a spectrofluorimeter (F-2000; Hitachi Sci. Instrs., Mountain View, CA). Relative F-actin content was determined by the ratio of the percent of emission of a cAMP-stimulated sample divided by the percent emission of unstimulated control samples.

Triton-insoluble Cytoskeletons

Triton-insoluble cytoskeletons were prepared according to Dharmawardhane et al. (1989). Cell lysates generated by this assay contain a final actin concentration near the critical concentration. These lysates are subjected to immediate centrifugation following cell lysis to avoid significant polymerization or depolymerization of cellular actin which may occur after lysis. Therefore, this assay is less influenced by changes in actin polymerization and is more sensitive to actin cross-linking. The actin content in the cytoskeletons was quantitated by scanning densitometry of the 42-kD actin band on Coomassie blue stained SDS-PAGE gels using a scanning densitometer (Molecular Dynamics, Sunnyvale, CA).

Confocal Microscopy

Cells were prepared for fluorescence microscopy according to Cox et al. (1992) with minor modifications. After starvation for 5.5 h in 14.8 mM NaH_2PO_4, 5.2 mM K_2HPO_4, pH 6.6 (20 mM Na/K/PO_4 buffer) the cells were treated with 3 mM caffeine and aliquots were allowed to settle on glow discharged polylysine (1 mg/ml of poly-L-lysine hydrobromide, mol wt >70,000) coated coverslips for 0.5 h before fixation. Cells were fixed either without stimulation (0 s) or 40–50 s after stimulation with 1 μM 2′ deoxy cAMP. Cells were also stained with rhodamine phalloidin to label F-actin. Stained slides were examined on a MRC-600 laser scanning confocal microscope (Bio Rad Labs., Hercules, CA), usually in the rhodamine/fluorescein two-channel configuration using the filter and mirror sets provided by Bio Rad. A Nikon 60× 1.4 numerical aperture planapochromat objective lens was used. Under our staining conditions the two channels were of approximately equal intensities in ABP-120$^+$ cells, where the same range of pixel values was obtained from the brightest section of each channel at the same pinhole and photomultiplier-gain settings. At these settings cross-talk between the two channels was at background levels. This was confirmed with the use of rhodamine-only and fluorescein-only stained control slides. The signal was of sufficient intensity that pinhole settings of five or less (Bio Rad) could be used in collecting image series in the Z axis. The optical slices were collected as the Kalman average of eight one-second scans. Under these conditions and with the optics used, the resolution of the x-y dimension was 0.3 μm and the z dimension was ~1.0 μm (Wells et al., 1990; Wilson et al., 1990).

Electron Microscopy

Cells in culture medium were allowed to adhere to ethanol cleaned and glow discharged polylysine-coated coverslips for 30 min. Non-adherent cells were washed off by carefully decanting the medium and replacing it with 20 mM Na/K/PO_4 buffer, pH 6.6. Adherent cells were starved on the coverslip for 5.5 h in 20 mM Na/K/PO_4 buffer. Cells were permeabilized for 2 min in DICTY PHEM buffer (15 mM Pipes, 6.25 mM Hepes, 10 mM EGTA, 0.5 mM $MgCl_2$, pH 6.9) containing 0.75% Triton X-100, 5 μM phallacidin, and protease inhibitors directly or after being exposed to 1 μM 2′ deoxy cAMP for 40 s. Cytoskeletons were fixed in DICTY PHEM buffer containing 2% glutaraldehyde (Polysciences Inc., Warrington, PA) for 15 min. The coverslips were extensively washed in glass-distilled water, rapidly frozen, freeze-dried, and rotary coated with 1.4 nm of tantalum-tungsten and 2.5 nm of carbon without rotation in a Cressington CFE-50 freeze-fracture apparatus (Cressington Scientific Instruments, Ltd., Watford, England) as described previously (Hartwig, 1992).

Labeling of Cytoskeletons with Myosin SI: Cytoskeletons were prepared by detergent permeabilization as above but before fixation they were incubated with 10 μM skeletal muscle myosin S1 in DICTY PHEM buffer for 10 min at room temperature, washed twice with DICTY PHEM buffer, and then fixed in 10 mM sodium phosphate buffer, pH 7.5, containing 0.2% tannic acid and 1% glutaraldehyde.

Gold Labeling for ABP-120: ABP-120 was localized in cytoskeletons using affinity-purified rabbit anti-ABP-120 IgG and 8-nm gold particles coated with goat anti-rabbit IgG in cytoskeletons from cells permeabilized and fixed with DICTY PHEM as described above. Before antibody labeling, unreacted aldehydes were blocked using a 5-min wash of 1 mg/ml sodium borohydride followed by washing thrice in PBS containing 1% BSA, pH 8.2. The cytoskeletons were incubated with 5 μg/ml of primary antibody for 60 min, washed thrice with PBS/BSA, incubated for 90 min with 8-nm gold particles coated with goat anti-rabbit IgG, washed thrice in PBS/BSA, thrice in PBS, and then fixed with 1% glutaraldehyde in PBS for 10 min. The cytoskeletons were washed in distilled water, rapidly frozen, freeze-dried, and metal-coated with tantalum-tungsten and carbon as described above.

Filament Lengths: The lengths of filaments present in cytoskeletons were determined as described previously by Neiderman et al. (1983).

Thickness of ABP-120⁻ and ABP-120⁺ Pseudopods

The cytoskeletal height of ABP-120⁻ and ABP-120⁺ pseudopods following stimulation was determined by the analysis of confocal and electron micrographs. Confocal images of the cells were obtained by staining cells for F-actin using rhodamine phalloidin. Polarized cells with a clear leading lamellipod that was attached to the coverslip were chosen for imaging. The thickness of an area 1 μm wide, either just inside the pseudopod or 3 μm inside the pseudopod, was determined from the number of Z-sections of known thickness that contained fluorescence. For the electron micrographs, the Z-axis height of filaments in cytoskeletons was determined from paired stereo micrographs as described previously (Hartwig and Shevlin, 1986).

Results

Polymerization of Actin and Its Incorporation into the Cytoskeleton Following cAMP Stimulation

Previous work has shown that in wild-type cells actin is polymerized in two waves in response to stimulation (Hall et al., 1988), an initial sharp peak at 10 s followed by a second less well-defined peak at 40–60 s. Actin becomes incorporated into the Triton X-100–insoluble cytoskeleton in three peaks, an initial sharp peak at 10 s and the second and third poorly resolved peaks between 30 and 60 s (Dharmawardhane et al., 1989). ABP-120 becomes incorporated into the cytoskeleton in two peaks that occur with the same kinetics as the second and third peaks of actin incorporation into the cytoskeleton suggesting that ABP-120 plays a role in the cross-linking of filaments into the cytoskeleton at these times (Dharmawardhane et al., 1989; Condeelis et al., 1990). In ABP-120–containing cells, pseudopod extension occurs in response to stimulation with cAMP during the second and third peaks of actin incorporation into the cytoskeleton. Therefore, the postulated sequence of events occurring in a narrow window of time following stimulation with cAMP is: actin polymerization, incorporation of ABP-120 into the cytoskeleton, ABP-120–mediated cross-linking of actin filaments, and then pseudopod extension. A causative relationship between ABP-120–mediated filament cross-linking and pseudopod extension is supported by the reduction in pseudopod extension from ABP-120⁻ cells between 30 and 60 s following stimulation (Cox et al., 1992).

To determine if the reduction in pseudopod extension following stimulation in ABP-120⁻ cells is correlated with defects in either actin polymerization or cross-linking of filaments into the cytoskeleton, two assays were carried out on identical populations of cells in parallel to distinguish these two events (Fig. 1). First, the amount of F-actin present in cells at various times before and following cAMP stimulation, in both ABP-120⁺ control and ABP-120⁻ cells, was determined using an NBD-phallacidin binding assay (Hall et al., 1988). The basal amount of F-actin in unstimulated ABP-120⁺ and ABP-120⁻ cells was the same, with values of 25.6 ± 5.4 and 25.8 ± 8.7 relative fluorescence units/10^6 cells for ABP-120⁺ and ABP-120⁻ cells, respectively (±SD from 5–7 experiments). There is no statistical difference in these values as indicated by a Student's *t* test with a P value of 0.96. Also, both the ABP-120⁺ and ABP-120⁻ cell lines polymerize the same amount of F- actin in response to cAMP (Fig. 1 *a*) and with the same kinetics even at times when pseudopods are normally extended following stimulation in ABP-120⁺ cells but fail to extend in ABP-120⁻ cells. *P* values at 10, 30, and 50 s were 0.689, 0.771, and 0.500, respectively, indicating that polymerization in ABP-120⁺ and ABP-120⁻ cells is not significantly different.

Second, the ability of the ABP-120⁺ and ABP-120⁻ cell lines to cross-link F-actin into the cytoskeleton was ana-

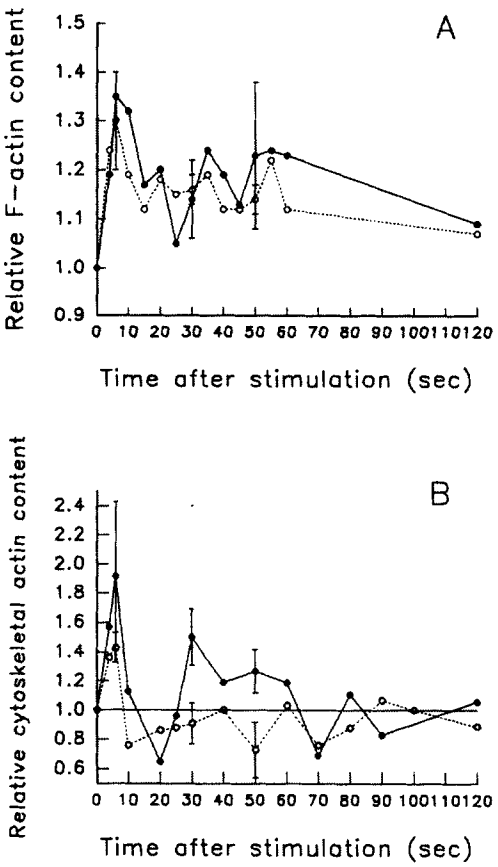

Figure 1 (*a*) Comparison of the kinetics of changes in total F-actin content following cAMP stimulation in ABP-120⁺ and ABP-120⁻ cells, as measured by NBD-phallacidin binding. Means for 2–6 values are shown. SEM (standard error of mean) is shown for T = 6, 30 and 50 s (n = 6). (*b*) Comparison of the kinetics of changes in relative actin content present in Triton X-100 insoluble cytoskeletons after stimulation with cAMP. Means for 2–7 values are shown. SEM for T = 6, 30 and 50 s are shown as in *a* (n = 7). (●) ABP-120⁺; (○) ABP-120⁻.

lyzed. Cells were lysed in Triton X-100 and the residue centrifuged gently so as to pellet only actin filaments that were cross-linked into the cytoskeleton at the time of cell lysis. The assay was done rapidly on ice to increase the sensitivity of the assay for cross-linking as described previously (Dharmawardhane et al., 1989). The ABP-120$^+$ control cell line showed the same kinetics of incorporation of actin filaments into the cytoskeletons as wild-type cells (wild type not shown). However, the ABP-120$^-$ cell line showed reduced actin incorporation into the cytoskeleton after stimulation at the times when ABP-120 is normally incorporated into the cytoskeleton and when pseudopods form in ABP-120$^+$ cells but fail to extend in ABP-120$^-$ cells (Fig. 1 *b*). That is, compared to ABP-120$^+$ cells, there is a significant decrease in the amount of F-actin incorporation into the cytoskeleton at 30 and 50 s in ABP-120$^-$ cells after stimulation, as shown by *t* test with *P* values of 0.038 and 0.050, respectively, while the 10 s peak of actin incorporation is unaffected by deletion of ABP-120 with a *P* value of 0.261.

By comparing Fig. 1, *a* and *b*, it is apparent that the defect in ABP-120$^-$ cells is not in the amount of F-actin present in resting cells or assembled between 30 and 50 s after stimulation with cAMP but in the ability of ABP-120$^-$ cells to incorporate F-actin into their cytoskeletons.

Confocal Microscopy

Fluorescence was recorded by confocal microscopy of cells that had adhered to polylysine-coated coverslips and then were fixed and stained for F-actin and ABP-120. The shapes of ABP-120$^+$ and ABP-120$^-$ cells both before and after stimulation with cAMP were studied. Although a variety of cell morphologies could be seen on each coverslip, the following generalizations can be made. Typical ABP-120$^+$ cells before and after stimulation with cAMP are shown in Figs. 2 and 3. ABP-120 is observed to be concentrated along with F-actin in surface projections in resting cells. After exposure to cAMP, ABP-120$^+$ cells (Fig. 3, row *1* and *2*) show an increased number of surface projections compared to ABP-120$^+$ cells that have not been stimulated (Fig. 2, row *1* and *2*) and these projections contain concentrations of ABP-120 and F-actin. In comparison, the ABP-120$^-$ cells show a reduced number of surface projections both before (Fig. 2, row *3*) and after stimulation with cAMP (Fig. 3, row *3*) when compared to ABP-120$^+$ cells. Staining with antibodies against ABP-120 in the ABP-120$^-$ cells was not observed (Fig. 3, row *4*) as demonstrated previously (Cox et al., 1992).

Confocal microscopy allows cells to be imaged in three dimensions. However, upon reconstruction, the conventional image produced is a view from directly above the cell. Using the volume rendering software VoxelView (Vital Images, Inc., Fairfield, Iowa), a cell image can be analyzed from various angles. This allows the dimensions of individual surface projections and pseudopods to be analyzed in the Z dimension. A greyscale intensity for each volume element (voxel) was used which is proportional to the fluorescence intensity in that region. Fig. 4 shows several different views of a volume reconstruction of the actin cytoskeleton of typical stimulated ABP-120$^+$ (Fig. 4 *b*) and ABP-120$^-$ (Fig. 4 *a*) cells, created from a Z-series of confocal microscope images of F-actin stained with rhodamine phalloidin. The ABP-120$^+$ cell has a greater number of projections over the entire surface of the cell in comparison to the ABP-120$^-$ cell. Both the ABP-120$^+$ and ABP-120$^-$ cells have lamellipodial projections in contact with the polylysine-coated coverslip. A leading lamellipod is seen in both the ABP-120$^+$ cell and the ABP-120$^-$ cell. However, when the leading lamellipods are viewed in profile (0°) it is apparent that the lamellipod in the ABP-120$^+$ cell is much thicker than the one seen in the ABP-120$^-$ cell. Quantitation of images (Table I) indicates that ABP-120$^+$ cells are approximately twice as thick as ABP-120$^-$ cells at the leading edge.

Electron Microscopy

Cytoskeletons from crawling *Dictyostelium* amoebae were prepared for electron microscopy in order to examine the structural differences in the ABP-120$^-$ cells that may underlie differences in behavior and dimensions of their projections observed in the light microscope, in comparison to the ABP-120$^+$ cells. Frontal lamellipodial areas of the cytoskeleton (within 5 μm from the front edge of the cell), identified from low magnification images, were examined from both unstimulated and cAMP-stimulated cells. Typical cytoskeletons for both unstimulated (0 s) and stimulated (40 s after cAMP) ABP-120$^+$ cells are shown in Fig. 5 and Fig. 8. These cytoskeletons display three features. First, as observed in the light microscope, pseudopods at the leading edge are very three-dimensional near the cytoskeletal edge (Table I). Second the actin filaments that compose the network are long, 1.18 μm $\pm$ 0.30 μm in length ($\pm$ SD, n = 100), and straight. In general, the bulk of the filaments run parallel to the substrate and cross one another at ~90° angles. A second set of filaments are oriented vertically to the substrate running from the cytoskeletal bottom to its surface. Third, filaments are organized into a space filling orthogonal network of high branching angles. This results in a contiguous network having pores of 50–100 nm in size. Bundles of filaments are present at the cell periphery and at the ventral surface of the lamellipods (Fig. 5, *black arrow*). Bundles interconnect and originate in the orthogonal filament network. Fig. 8 shows that these three features are conserved in cytoskeletons from cells stimulated with cAMP before detergent permeabilization. The *Dictyostelium* cortical cytoskeleton is therefore structurally identical to that of macrophage cytoskeletons except that the filaments composing the networks of *Dictyostelium* are longer (Hartwig and Shevlin, 1986).

The biochemical evidence in Fig. 1 suggests that ABP-120 cross-links filaments into the cytoskeleton during pseudopod formation. To determine if ABP-120 is present throughout the volume of the pseudopodial network and located at sites

Figure 2. Confocal fluorescence micrographs of unstimulated ABP-120$^+$ and ABP-120$^-$ cells. (Row *1*) Pseudo-phase contrast image of a typical ABP-120$^+$ cell and corresponding stereo pair of F-actin stained with rhodamine phalloidin. (Row 2) Stereo pair of the same cell as in (row *1*) stained for the presence of ABP-120. (Row *3*) Pseudo-phase contrast image of a typical ABP-120$^-$ cell and corresponding stereo pair showing F-actin. Bar, 10 μm.

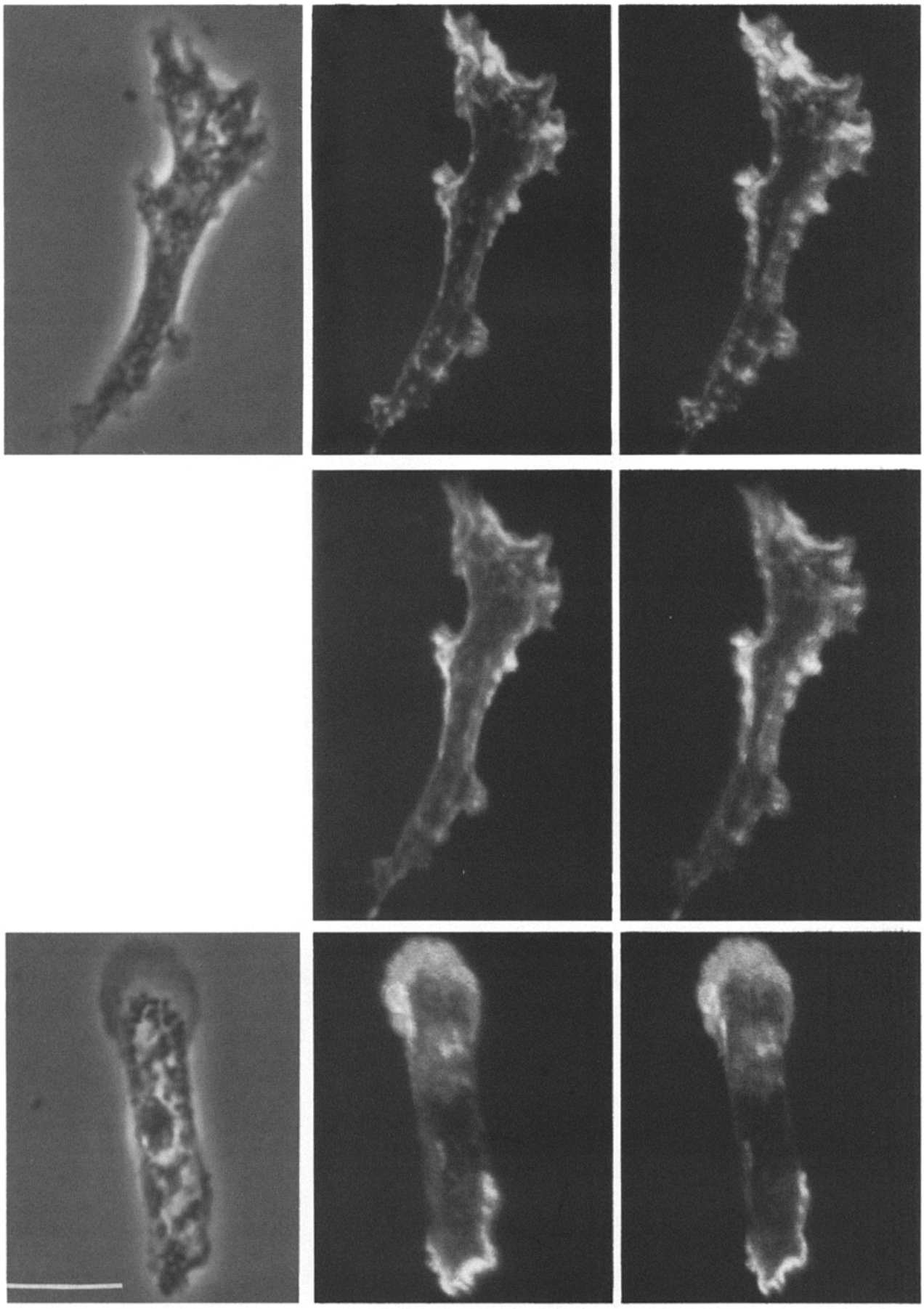

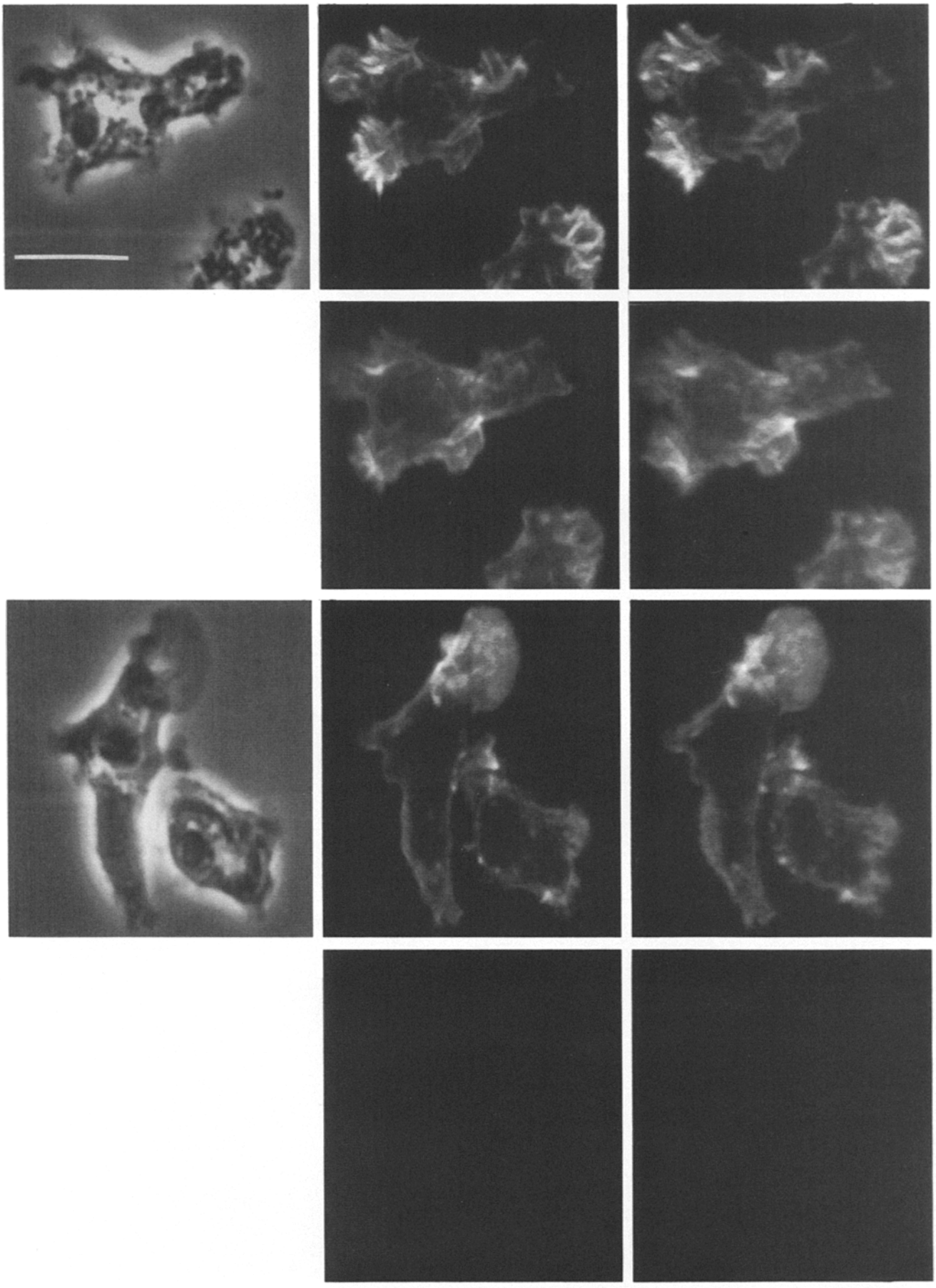

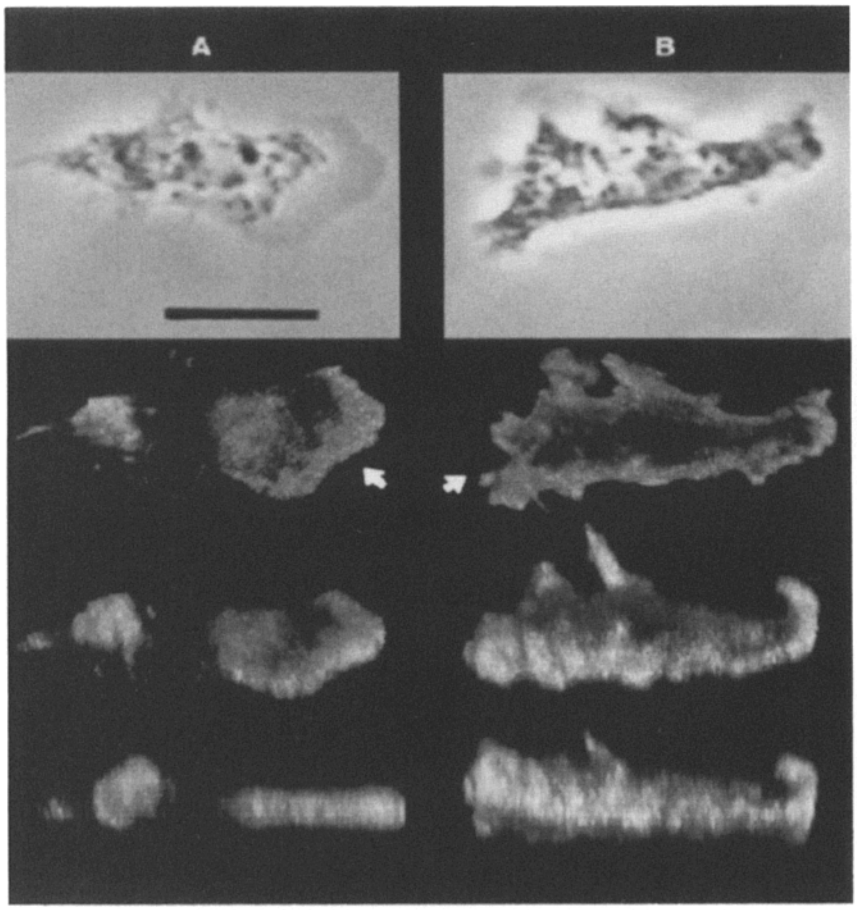

Figure 4. 3D volume rendering of the F-actin fluorescence images of a typical (*a*) ABP-120$^-$ cell and (*b*) ABP-120$^+$ cell after stimulation with cAMP (40 s). Views shown are (from top to bottom) pseudo-phase contrast 90°, 45°, and 0° (edge-on). The leading edge of each cell is shown by the arrowhead. Bar, 10 μm.

where actin filaments interact the location of ABP-120 in the filament network of ABP-120$^+$ cells was determined by immunoelectron microscopy. Fig. 7 shows the location of ABP-120 as visualized with anti-ABP-120 IgG and 8-nm colloidal gold particles. ABP-120 is dispersed throughout the volume of the pseudopod in association with filaments. Stereo viewing also reveals precise information on the location of ABP-120 with regard to actin. Gold labeling predominates at filament intersection points indicating that ABP-120 is found at places where actin filaments interact. There were no gold particles found in ABP-120$^-$ networks prepared under the same conditions (data not shown).

Actin filaments in similar regions of the cytoskeleton have a different organization in ABP-120$^-$ cells when compared

Table I. Thickness of ABP-120$^-$ and ABP-120$^+$ Pseudopods

Distance from cytoskeletal margin	ABP-120$^-$ cytoskeletal height	ABP-120$^+$ cytoskeletal height	*t* Test *P* value
	μm ± SEM (n)		
Determined from confocal Z series			
edge–1 μm	1.8 ± 0.1 (20)	3.4 ± 0.4 (14)	<0.001
3 μm	2.1 ± 0.2 (10)	3.7 ± 0.4 (14)	<0.001
Determined from electron micrographs			
edge	0.32 ± 0.05 (10)	0.87 ± 0.11 (10)	<0.001
1 μm	0.38 ± 0.04 (10)	0.78 ± 0.07 (10)	<0.001
2 μm	0.40 ± 0.04 (10)	0.99 ± 0.07 (10)	<0.001
3 μm	0.50 ± 0.05 (10)	1.23 ± 0.11 (10)	<0.001

Figure 3. Confocal fluorescence micrographs of typical ABP-120$^+$ and ABP-120$^-$ cells after stimulation with 1 μM 2′ deoxy cAMP. (Row *1*) Pseudo-phase of typical ABP-120$^+$ cells and corresponding stereo pair of F-actin stained with rhodamine phalloidin. (Row *2*) Stereo pair of the same cells as in (Row *1*) stained for the presence of ABP-120. (Row *3*) Pseudo-phase of a typical ABP-120$^-$ cell and corresponding stereo pair showing F-actin. (Row *4*) Stereo pair of the same cells as in (row *3*) stained for ABP-120. Cells were prepared and imaged under identical conditions to those shown in Fig. 2. Bar, 10 μm.

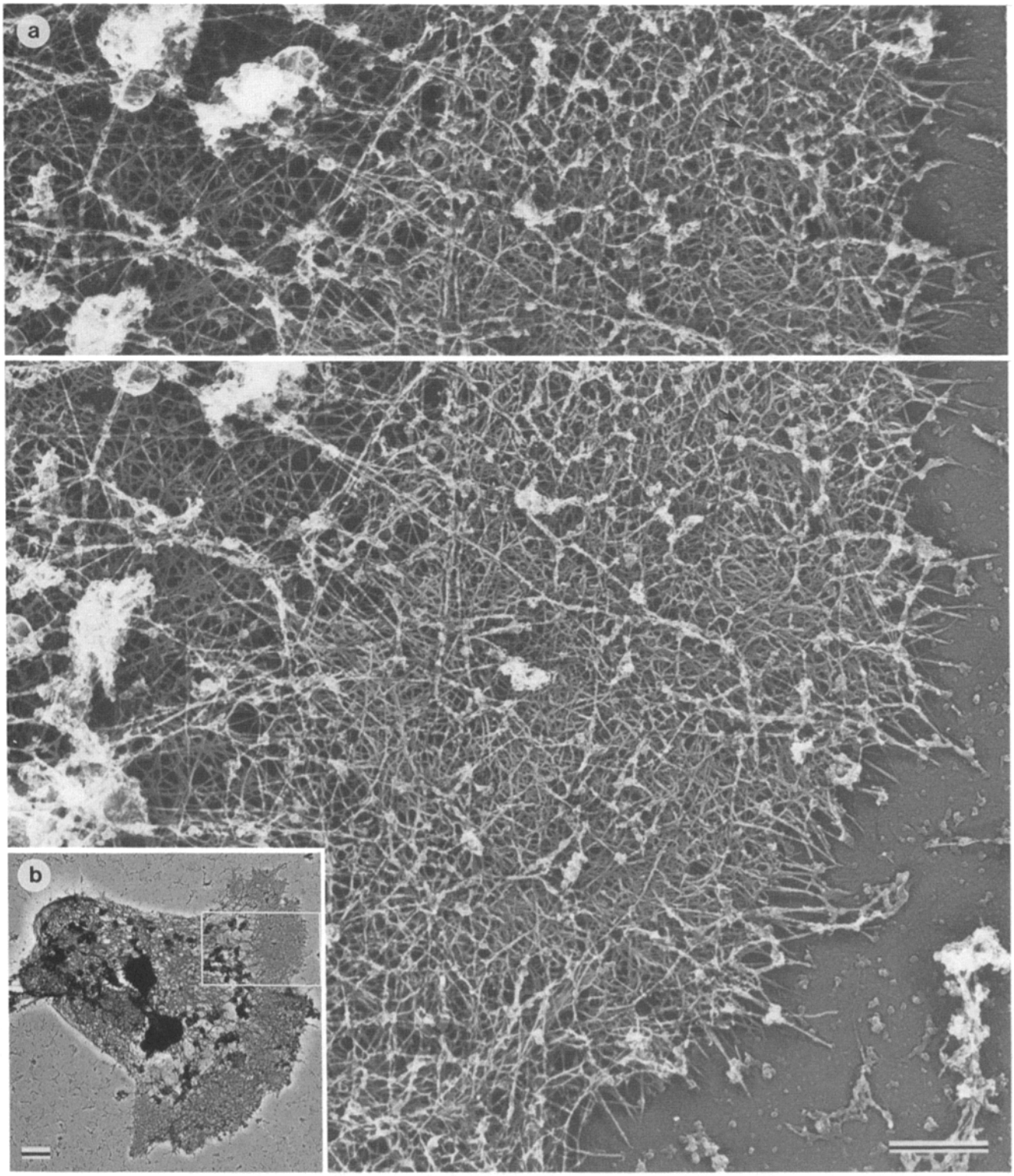

Figure 5. Structure of the cytoskeleton from a representative unstimulated ABP-120$^+$ cell that was crawling on a polylysine-coated glass coverslip before detergent permeabilization. (*a*) Paired electron micrographs show the typical lamellipodial filament network of this unstimulated ABP-120$^+$ cell. The lamellipod is composed of actin filaments, 1.0- 2.0 μm in length, ordered into a dense orthogonal network. Bundles of actin filaments are observed. They appear to form when filaments running from the network coalesce into parallel arrays (*black arrow with white edges*). To obtain a stereo image, turn the micrographs 90° clockwise and view the right half of the micrograph. (*b*) Low magnification image of the entire cell identifying the region shown in *a*. This is the cytoskeleton from a cell that had a broad frontal lamellipod extending 3–5 μm from the cell body. Bars: (*a*) 500 nm; (*b*) 2 μm.

to the ABP-120$^+$ cells. Typical cytoskeletons from unstimulated and stimulated ABP-120$^-$ cells are shown in Figs. 6 and 9. The networks of ABP-120$^-$ cells are much less three dimensional (Table I) and have smaller pore sizes than networks of ABP-120$^+$ cells both before and after stimulation. The filaments are not as straight and lie as a flat mat on the ventral cell surface. Close inspection reveals the presence of foci of aggregated filaments within the cortical lamellae (Figs. 6 *c* and 9, *arrows*). These foci are usually found near the bottom of the cytoskeleton and are never seen in ABP-120$^+$ cells.

To rule out the possibility that ABP-120$^-$ cells were forming filamentous structures that were not actin filaments, the filaments of both ABP-120$^+$ and ABP-120$^-$ networks were labeled with myosin S1. Filaments in both cell types labeled with S1 give the arrowhead pattern diagnostic of actin filaments. The filaments are randomly oriented in both ABP-120$^+$ and ABP-120$^-$ networks as seen by the random orientation of the barbed ends of the filaments (Fig. 10). Once again the actin network of the ABP-120$^-$ cell shown in Fig. 10 *b* is less three-dimensional and filaments are more intertangled than that of the ABP-120$^+$ networks (Fig. 10 *a*).

Discussion

ABP-120$^-$ Cells Respond to cAMP by Polymerizing Actin but Fail to Incorporate Actin into the Cytoskeleton

An important issue that remained unresolved after previous analyses of ABP-120$^-$ mutants was the cause of the reduction in cytoskeletal actin in ABP-120$^-$ cells after stimulation of motility with cAMP (Cox et al., 1992). The reduction could result from diminished actin polymerization, increased depolymerization, or failure of mutants to cross-link filaments into the cytoskeleton. The present study using ABP-120$^+$ control transformants and ABP-120$^-$ cells derived from the same AX3 strain of *Dictyostelium* resolves this issue. The kinetics of actin polymerization and depolymerization following stimulation by cAMP is identical to both the ABP-120$^+$ and ABP-120$^-$ cells: both cell populations increase their actin filament content by 25–30% after exposure to cAMP. However, the ABP-120$^-$ cells do not shown a corresponding increase in incorporation of actin into the cytoskeleton at times corresponding to the second and third peaks of incorporation in wild-type cells. Therefore, the reduction of cytoskeletal actin results not from a change in their capacity to polymerize actin but from an inability of the ABP-120$^-$ cells to cross-link F-actin into the cytoskeleton beginning 30 s after stimulation. This deficit is significant since the second and third peaks of incorporation of actin into the cytoskeleton are temporally correlated with pseudopod extension.

Furthermore, the observation that the first peak of incorporation of actin into the cytoskeleton following stimulation with cAMP is unaffected in ABP-120$^-$ cells indicates that cross-linking of actin by ABP-120 is not required at this time. This is consistent with the kinetics of incorporation of ABP-120 into the cytoskeleton in wild-type cells which indicate that ABP-120 does not bind to the cytoskeleton during the first peak but does bind during the second and third peaks of actin incorporation into the cytoskeleton (Dhamawardhane et al., 1989). Taken together, these results suggests a causative relationship between ABP-120–mediated filament cross-linking and pseudopod extension.

Lamellipods from ABP-120$^-$ Cells have Altered Three Dimensional Morphologies and Filament Packing

Dictyostelium amoebae spread and crawl over polylysine-coated glass surfaces and, after exposure to cAMP, both the ABP-120$^+$ and ABP-120$^-$ cells increase their protrusive activity when compared to unstimulated cells. ABP-120$^-$ cells, however, exhibit much less protrusive activity both before and after stimulation with cAMP compared to the ABP-120$^+$ cells (Cox et al., 1992) and lamellipods produced by the ABP-120$^-$ cells are not as large or thick as those extruded by ABP-120$^+$ cells. Comparison of images from both the confocal and electron microscope revealed clear differences in the thickness of these lamellae with ABP-120$^-$ cells having much flatter projections. Both techniques show a similar difference in pseudopod thickness between ABP-120$^+$ and ABP-120$^-$ cells. The absolute value of pseudopod thickness as measured by these two techniques is different due to spherical aberration in the confocal microscope, which distorts the Z-axis. This phenomenon is caused by having mismatched refractive indices in an optical system, such as between the oil, coverslip, mounting media, and the specimen itself. Spherical aberration increases proportionally with depth into the aqueous media and specimen and can alter morphological data. Due to spherical aberration, reconstruction of a Z-series of a perfectly round object will result in an oval, elongated in the Z-axis (Visser et al., 1992; Hell et al., 1993; Brenner, 1994).

To investigate the cause of these morphological alterations in pseudopod size, rapidly frozen, freeze-dried, and metal-coated cytoskeletons were viewed in the electron microscope. Micrographs of lamellipods at the leading edges of cytoskeletons of ABP-120$^+$ cells revealed orthogonal actin filament networks interspersed with occasional actin filament bundles. We concentrated here on the structure of the network because as discussed below this structure shows the greatest modification in the ABP-120$^-$ cells. In ABP-120$^+$ cells, lamellipods appear to find support in a space filling orthogonal network assembled from long, straight actin filaments. Most of the filaments of this network run in parallel with the glass substratum, fanning out centrifugally from the interior margin of the lamellae, and cross one another at near 90° angles. Other filaments run vertically up from the substrate and appear to be "tent poles" on which the other filaments draw support. This filament geometry results in an efficient three-dimensional structure capable of filling maximal volume with minimal amounts of filaments and is consistent with the observation that cross-linking of F-actin by ABP-120 in vitro leads to orthogonal networks with regular filament spacing and the consistency of a rigid gel (Niedermann et al., 1983; Condeelis et al., 1984; Wolosewick and Condeelis, 1986). Thus, ABP-120 molecules, located specifically in this network at points of filament intersection (Fig. 7), are likely to rigidify the network by cross-linking the filaments.

By direct comparison to ABP-120$^+$ cells, the actin cortex of ABP-120$^-$ cytoskeletons appears denser, thinner, and the

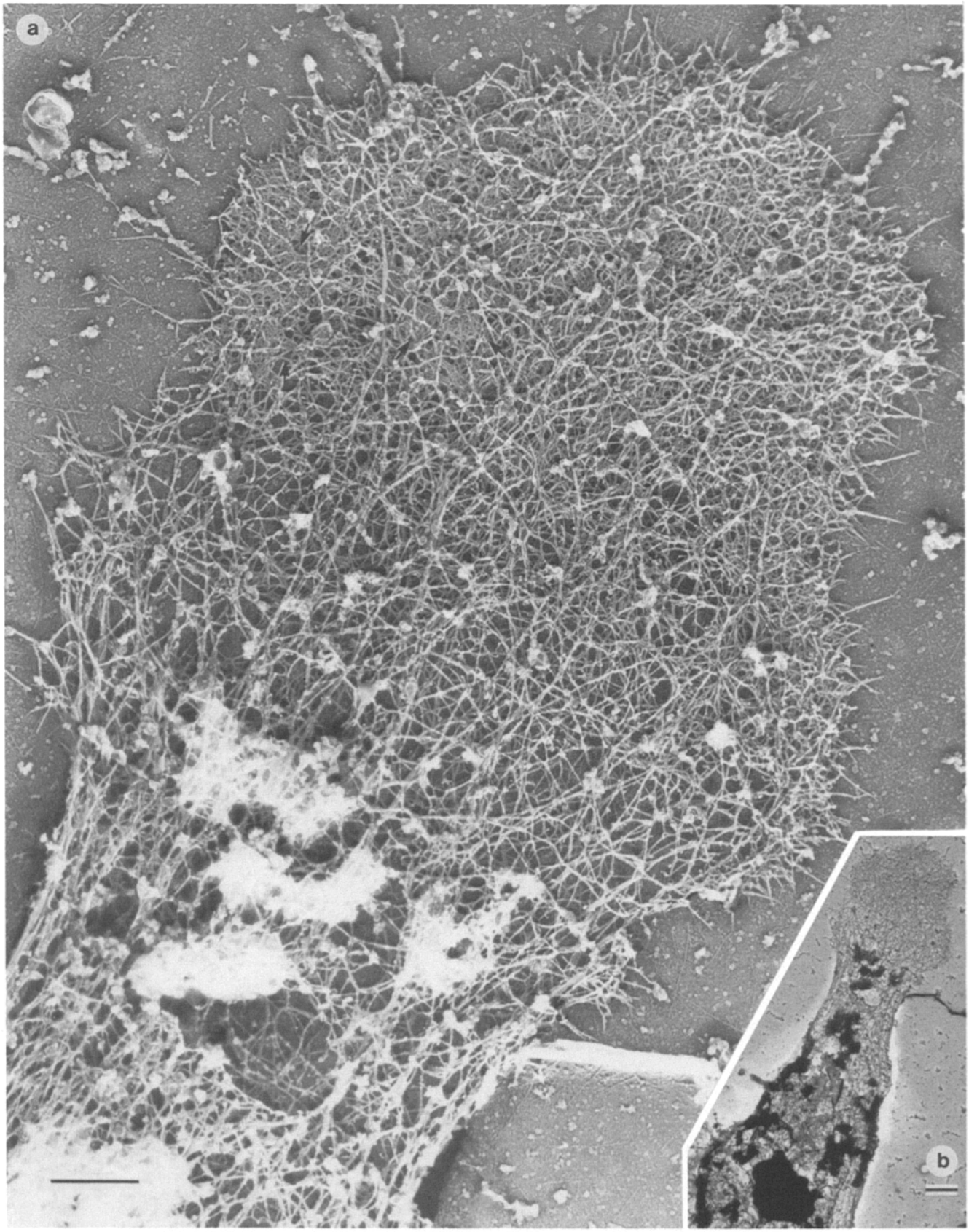

Figure 6. Structure of a cytoskeleton from a representative unstimulated ABP-120$^-$ cell crawling on a polylysine-coated glass coverslip prior to detergent permeabilization. ABP-120$^-$ cells extend smaller and flatter pseudopods than ABP-120$^+$ cells (compare with Figs. 5 and 8). (*a*) Actin filaments composing the pseudopods are curled and intertangled. Large, flat aggregates of actin filaments are apparent (*black arrows with white edges*). These aggregates are shown in stereo in *c*. (*b*) Low magnification view of the cytoskeleton. (*c*) Paired electron micrographs showing region of the cytoskeleton of the cell shown in *a*. Stereo viewing reveals that this frontal pseudopod is relatively flat. Large tangles of actin filaments are present at the bottom of the cytoskeleton at many points (*black arrows with edges*). Bars: (*a*) 500 nm; (*b*) 1 μm; (*c*) 100 nm.

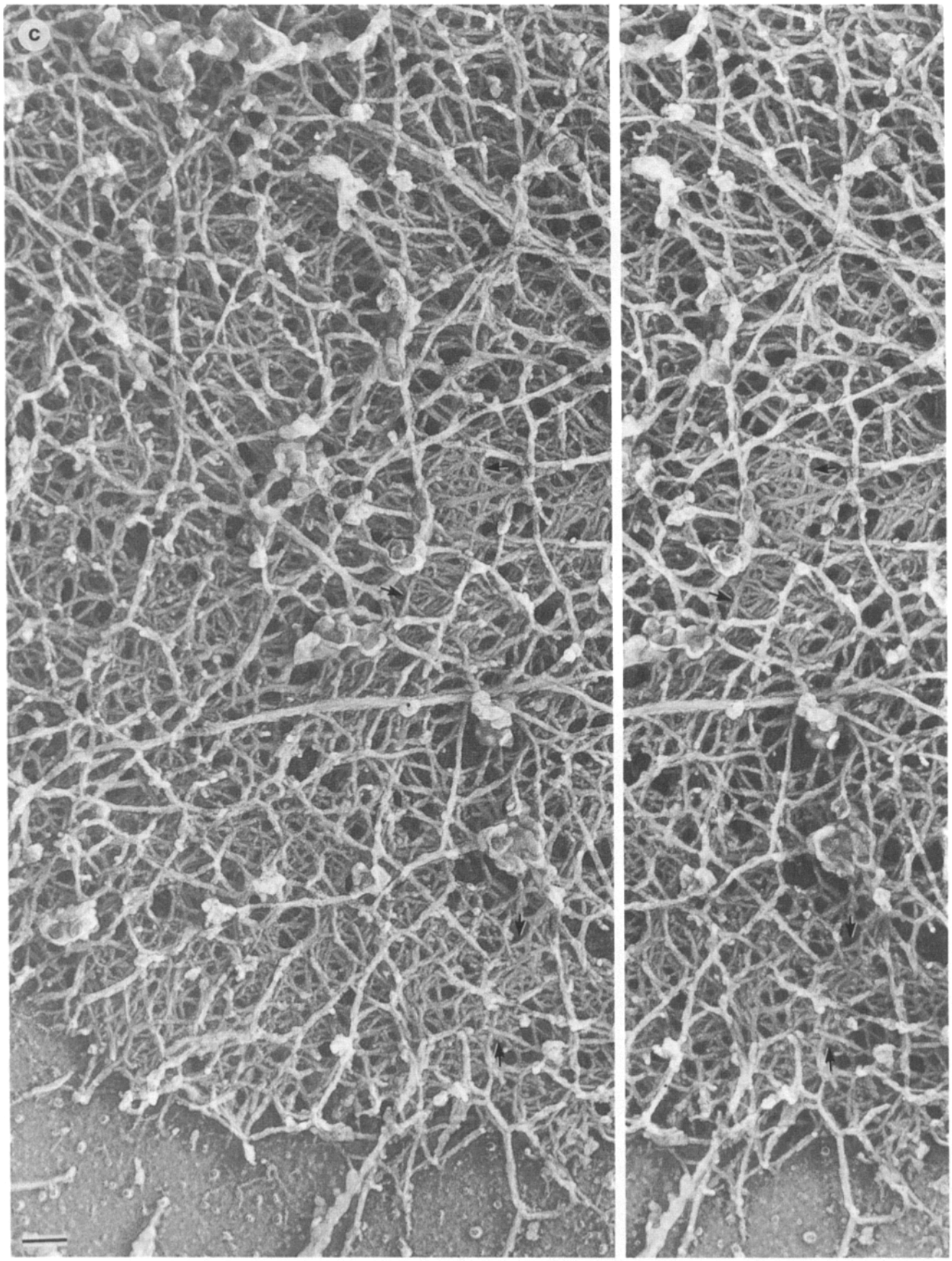
C

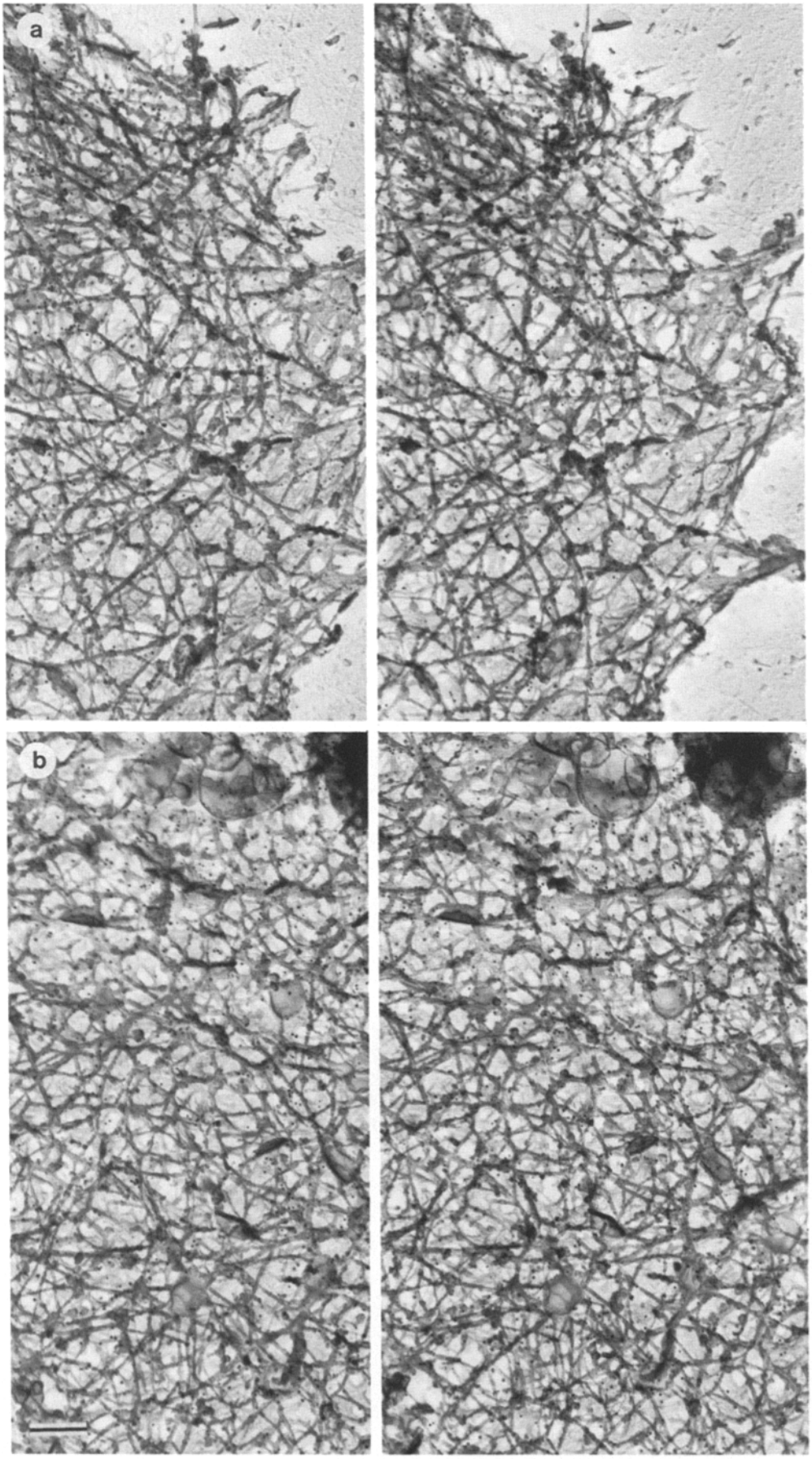

Figure 7. Location of ABP-120 in the peripheral cytoskeleton of *Dictyostelium.* ABP-120 is located throughout the lamellipodial network using affinity-purified rabbit anti-*Dictyostelium* ABP-120 IgG and 8-nm gold particles coated with goat anti-rabbit IgG. Paired electron micrographs show two different regions at the cytoskeletal periphery. ABP-120 locates throughout the volume of the actin filaments composing the cytoskeletal periphery, particularly at filament intersection points. Bar, 200 nm.

interfilament distance is less regular. In many areas, the cortex contains foci of aggregated actin filaments near the ventral cell surface indicating that the absence of ABP-120 results in loss of regular interfilament spacing and orthogonality between filaments. These comparative observations are consistent with the findings that ABP-120$^-$ cells are defective in cross-linking of actin into the cytoskeleton during pseudopod extension (Fig. 1).

These results indicate that ABP-120 is required for the cross-linking of actin filaments in pseudopods to form a space filling orthogonal network with the consistency of a rigid gel. Furthermore, the observations that pseudopods in ABP-120$^-$ cells are flatter, smaller (Fig. 4, Table I), and extended more slowly than in ABP-120$^+$ cells (Cox et al., 1992) indicate that formation of a rigid orthogonal network of filaments, as mediated by proteins like ABP-120, is required for normal pseudopod extension as discussed in detail elsewhere (Condeelis, 1993*a*; Oster, 1984).

Comparison of the Organization of Actin in Lamellae of Rapidly Motile Phagocytes

Dictyostelium amoebae and mammalian leukocytes are highly motile cells that can move at velocities in excess of 10 μm/min. Rapid locomotion is accompanied by, and thought to require, the extension of large lamellipods that are densely filled with actin filaments. Since the mode of motility and behavior of these phagocytes are very similar, comparisons of the three-dimensional structure and biochemical composition of the actin cytoskeleton in lamellae of these cell types is useful because it may provide insights into the mechanics of pseudopod extension and motility. In this study, for the first time, the three-dimensional structure of the lamellipodial actin cytoskeletons of *Dictyostelium* has been visualized using rapid-freezing, freeze-drying, and rotary coating in a way identical to that used with mammalian white cells to allow direct comparison of the lamellar cytoskeleton of *Dictyostelium* and leukocytes. In both cell types, networks of orthogonally oriented actin filaments fill the volume of the lamellipods of *Dictyostelium* and leukocytes. These networks have the mechanical advantage of occupying the maximum volume with minimal polymer mass. Furthermore, actin filaments approach the plasma membrane with either filament end and laterally in *Dictyostelium* as reported previously for the lamellar cytoskeleton of macrophages and neurons (Hartwig and Yin, 1988; Lewis and Bridgeman, 1992, respectively).

In comparison to macrophages and platelets, filaments forming the lamellar networks of *Dictyostelium* are long, with filament lengths of 1–2 μm discernible. This is in contrast to the filament length distribution determined biochemically for the entire *Dictyostelium* cytoskeleton (Podolski and Steck, 1990) and longer by a factor of two to three than the actin filaments in the cortex of macrophage cytoskeletons. The difference in filament length observed here does not result from the loss of a large population of short filaments or to depolymerization of filaments since small soluble nuclei (i.e., short free filaments) are not detected in nucleation assays of *Dictyostelium* (Hall et al., 1989) and permeabilization solutions used in this study contained phallacidin concentrations in molar excess to that of actin. A possible explanation for differences in filament length distribution in *Dictyostelium* is that different populations of filaments were sampled. The filament length distribution measured biochemically by Podolski and Steck (1990) was for the entire *Dictyostelium* cell and sampled filaments in relatively inactive regions of the cell cortex where filaments are expected to be short. In our study only filaments in growing pseudopods where actin polymerization is occurring (Hall et al., 1988) were visualized and are, therefore, expected to be longer than in inactive regions of the cell cortex.

In macrophages, the high molecular weight ABP-280 has been implicated in generating networks of orthogonal filaments (Hartwig and Shevlin, 1986; Hartwig and Yin, 1988) as well as linking filaments and the network to the plasma membrane (Ohta et al., 1991). In *Dictyostelium*, the smaller protein, ABP-120, which is related to ABP-280 and shares many of the same structural features, has been implicated in generating networks of orthogonally arranged actin filaments (Wolosewick and Condeelis, 1986). Both proteins reside at filament branch points in networks in situ (Fig. 7; Hartwig and Shevlin, 1986). This suggests that ABP-120 and ABP-280 have similar functions in vivo and that the entire tail portion of ABP-280, which is much longer than that of ABP-120, is not required for the cross-linking of filaments into orthogonal geometries as seen in situ. However, this conclusion is complicated by the existence of an ABP-280–related protein in *Dictyostelium* amoebae called ABP-240 (Hock and Condeelis, 1987; Condeelis et al., 1988). ABP-240 has hydrodynamic, immunological, and morphological properties similar to the ABP-280/filamin family of proteins. ABP-240 is a potent actin filament cross-linker and is present in lamellipods of *Dictyostelium* (Ridsdale, unpublished observations) suggesting that ABP-240 may contribute to the final geometries of filaments in networks observed in *Dictyostelium* lamellipods.

The Cortical Expansion Model

The cortical expansion model for pseudopod extension proposes three essential steps for pseudopod formation: (*a*) the local polymerization of actin is followed by (*b*) cross-linking of these filaments to form a space filling gel, (*c*) the further expansion of which leads to pseudopod extension. Gel expansion can result from either polymerization and cross-linking of filaments within the gel, and/or gel osmotic force where the relative contribution of each would depend on the geometry of filaments in the gel. For example, actin polymerization and cross-linking are probably sufficient for elongation of filopods where filaments are cross-linked into bundles. While, in addition to polymerization and cross-linking, gel osmotic force is probably required for the expansion of orthogonal filament networks as described previously (Oster and Perelson, 1983; Oster, 1984; Condeelis, 1993*a*). Increases in the volume of gelled networks of actin filaments by gel osmotic force requires a reduction in the elastic modulus of the gel during water uptake (Oster, 1984) which can occur through the severing action of proteins like gelsolin and severin. Any model for the generation of protrusive force that uses filament polymerization and cross-linking does not require myosin-mediated filament sliding either directly in the pseudopod as in the frontal contraction model or indirectly during the generation of hydrostatic pressure as in the tail contraction model, as described previously (Con-

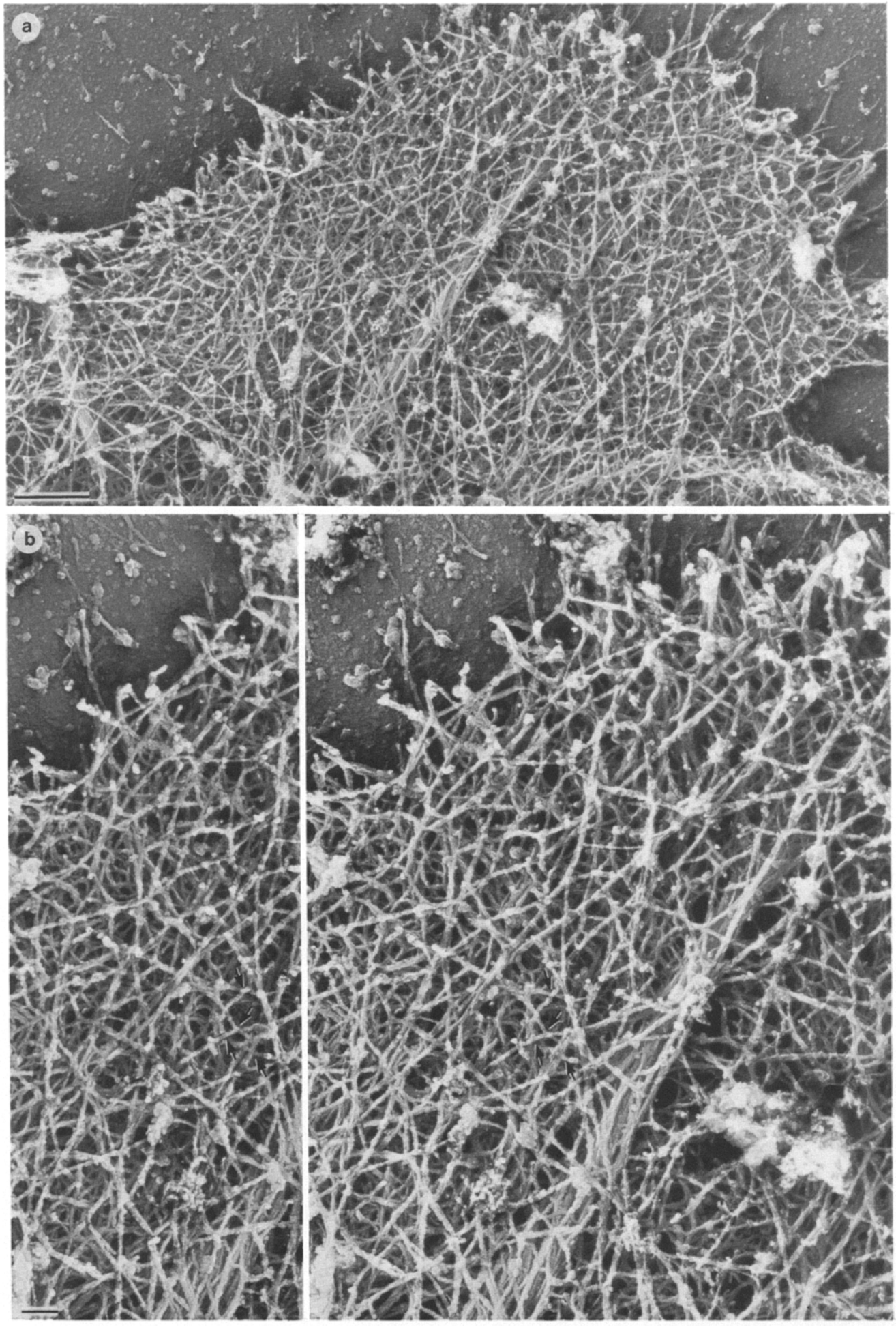
a
b

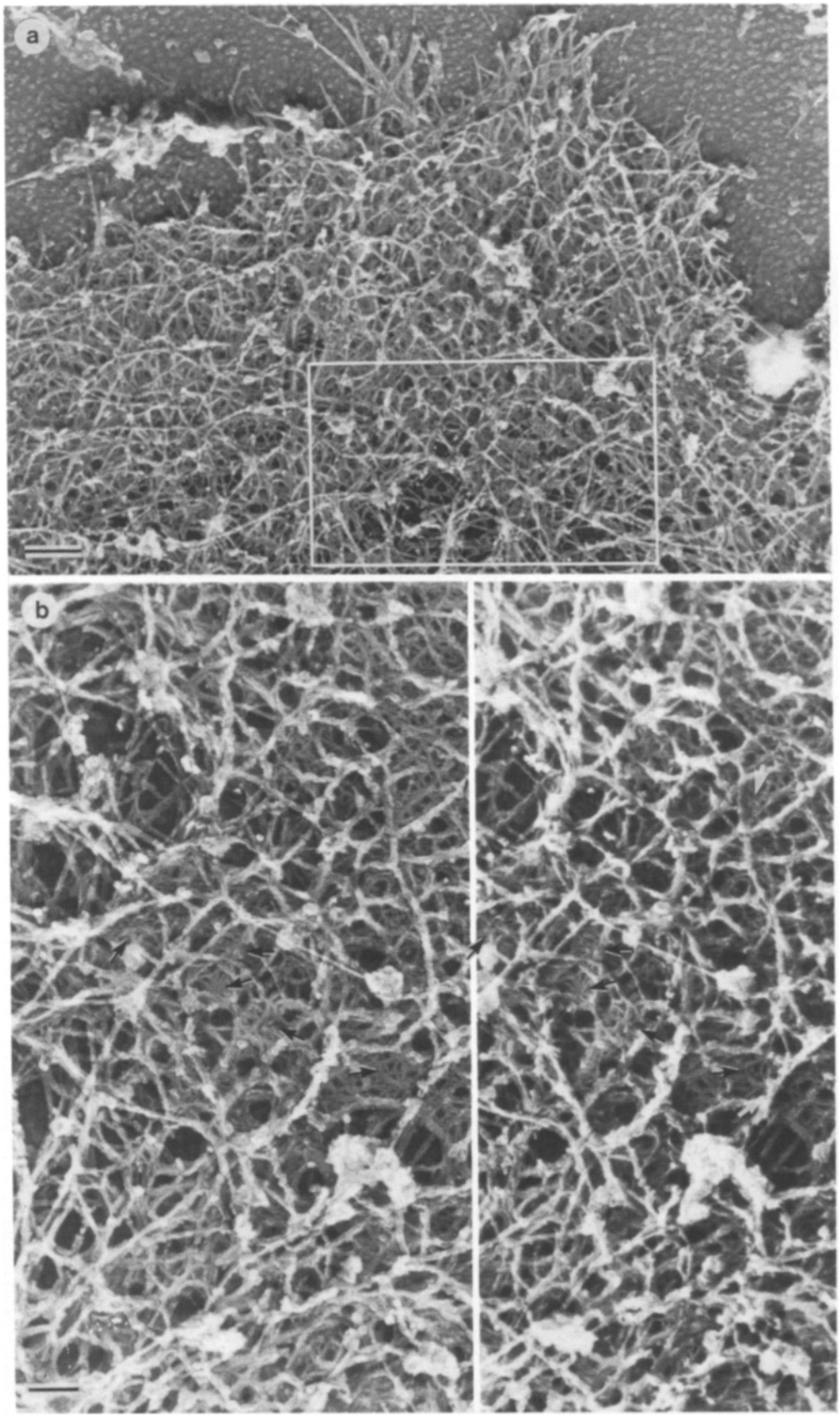

Figure 9. Actin filament structure in a lamellipod of a ABP-120$^-$ cytoskeleton from a cell crawling on polylysine coated glass and then stimulated with cAMP for 40 s. (*a*) Lamellipods for ABP-120$^-$ cytoskeletons are flat and contain aggregates of actin filaments. (*b*) Structure of filament aggregates in ABP-120$^-$ cytoskeletons. Some of the filament aggregates are indicated with black arrows with white edges. Bars: (*a*) 300 nm; (*b*) 100 nm.

Figure 8. (*a*) Representative pseudopod from a cytoskeleton of an ABP-120$^+$ cell crawling on a glass coverslip and then stimulated with cAMP for 40 s before detergent permeabilization. This pseudopod shares the features of pseudopods from the unstimulated ABP-120$^+$ cells in that it is composed of long filaments, many which run the entire length of the pseudopod (~2.5–3 μm). A large actin filament bundle runs along the bottom (ventral surface) of the cytoskeleton. As in the unstimulated cell, the bulk of the actin filaments are organized into a highly branched network. (*b*) Paired electron micrographs showing a portion of the pseudopod in *a*. By comparison to Fig. 5, this pseudopod is a thicker structure. Some filaments interconnect end-to-side to form perpendicular connections or intersect and cross at ~90° (a few intersections are indicated by the *black arrows with white edges*). Many filament pairs are observed but they are also arrayed in an orthogonal network. Bars: (*a*) 500 nm; (*b*) 100 nm.

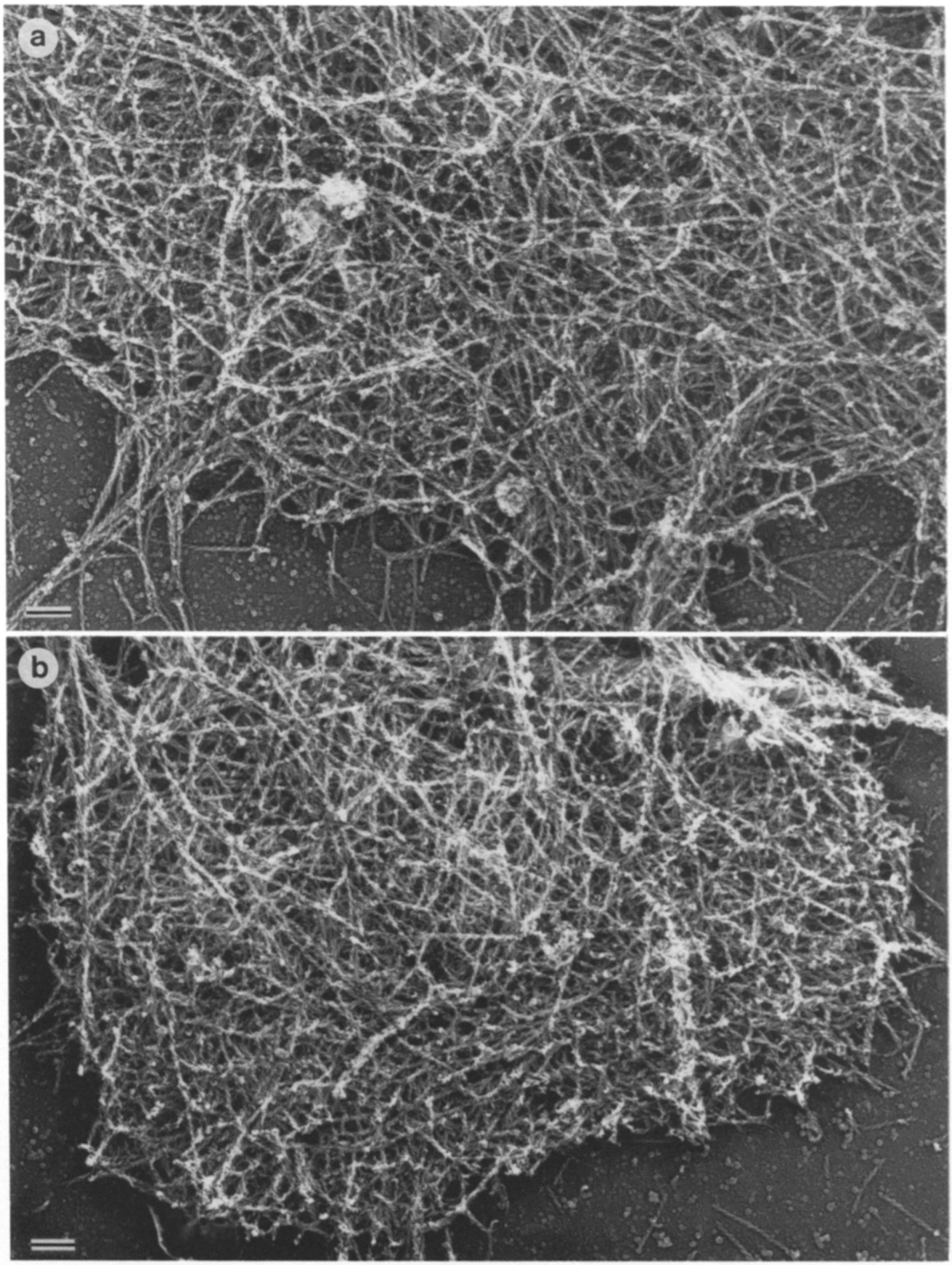

Figure 10. The filaments composing the lamellipodial networks of both ABP-120$^+$ (*a*) and ABP-120$^-$ cytoskeletons (*b*) are actin. Actin filaments were identified by labeling them with myosin S1. As was observed in the unlabeled cytoskeletons, the actin filaments that compose the orthogonal networks of the ABP-120$^+$ cytoskeletons are long and straight. By comparison, the periphery of ABP-120$^-$ cytoskeletons have a dense matte of intertangled actin filaments. Bar, 200 nm.

deelis, 1992). The Cortical Expansion hypothesis predicts that the essential intermediate step in protrusive activity is filament cross-linking not sliding, and this is supported by both the observations reported here and in previous analyses of cell lines defective in the expression of ABP-120 which cannot extend pseudopods normally (Cox et al., 1992). Furthermore, studies of mutant cell lines defective in the expression of myosin II (Wessels et al., 1988) and various isoforms of myosin I (Wessels et al., 1991; Titus et al., 1993) demonstrate that these abundant isoforms of myosin are not required for pseudopod extension.

The authors are grateful to the reviewers for their help in strengthening the manuscript and to the members of the Condeelis lab for editorial comments. The authors would also like to thank the Image Analysis Facility at the Albert Einstein College of Medicine for use of the confocal microscope.

This study was supported by National Institutes of Health grants GM25813 (J. Condeelis), HL47874 (J. Hartwig), and training grant 5T32 HL07675-03 (D. Cox).

Received for publication 13 September 1994 and in revised form 7 December 1994.

References

Brenner, M. 1994. Imaging dynamic events in living tissue using water immersion objectives. *American Lab. (Shelton)* 26(6):14–19.

Bresnick, A. R., V. Warren, and J. Condeelis. 1990. Identification of a short sequence essential for actin binding by *Dictyostelium* ABP-120. *J. Biol. Chem.* 265:9236–9240.

Bresnick, A. R., P. A. Janmey, and J. Condeelis. 1991. Evidence that a 27-residue sequence is the actin binding site of ABP-120. *J. Biol. Chem.* 266:12989–12993.

Brink, M., G. Gerish, G. Isenberg, A. A. Noegel, J. E. Segall, E. Wallraff, and M. Schleicher. 1990. A *Dictyostelium* mutant lacking and F-actin cross-linking protein, the 120-kD gelaton factor. *J. Cell Biol.* 111:1477–1489.

Carboni, J. M., and J. S. Condeelis. 1985. Ligand-induced changes in the location of actin, myosin, 95 K (α-actinin), and 120 K protein in amebae of *Dictyostelium discoideum*. *J. Cell Biol.* 100:1884–1893.

Condeelis, J. 1981. Microfilament-membrane interactions in cell shape and surface architecture. *In* International Cell Biology 1980-1981. H. G. Schweiger, editor. Springer-Verlag, Berlin. 306–320.

Condeelis, J. 1992. Are all pseudopods created equal? *Cell Motil. Cytoskeleton.* 22:1–6.

Condeelis, J. 1993*a*. Life at the leading edge: the formation of cell protrusions. *Annu. Rev. Cell Biol.* 9:411–444.

Condeelis, J. 1993*b*. Understanding the cortex of crawling cells: insights from *Dictyostelium*. *Trends Cell Biol.* 3:371–376.

Condeelis, J., M. Vahey, J. M. Carboni, J. DeMey, and S. Ogihara. 1984. Properties of the 120,000- and 95,000-dalton actin binding proteins from *Dictyostelium discoideum* and their possible functions in assembling the cytoplasmic matrix. *J. Cell Biol.* 99:119s–126s.

Condeelis, J., S. Ogihara, H. Bennet, J. Carboni, and A. Hall. 1987. Ultrastructural localization of cytoskeletal proteins in *Dictyostelium* amoebae. *Methods Cell Biol.* 28:191–207.

Condeelis, J., A. Hall, A. Bresnick, V. Warren, R. Hock, H. Bennet, and S. Ogihara. 1988. Actin polymerization and pseudopod extension during amoeboid chemotaxis. *Cell Motil. Cytoskeleton.* 10:77–90.

Condeelis, J., A. Bresnick, M. Demma, S. Dharmawardhane, R. Eddy, A. L. Hall, R. Sauterer, and V. Warren. 1990. Mechanisms of amoeboid chemotaxis: an evaluation of the cortical expansion model. *Dev. Genet.* 11:333–340.

Cooper, J., 1991. The role of actin polymerization in cell motility. *Annu. Rev. Physiol.* 53:585–605.

Cox, D., J. Condeelis, D. Wessels, D. Soll, H. Kern, and D. Knecht. 1992. Targeted disruption of the ABP-120 gene leads to cells with altered motility. *J. Cell Biol.* 116:943–955.

Dharmawardhane, S., V. Warren, A. L. Hall, and J. Condeelis. 1989. Changes in the association of actin binding proteins with the actin cytoskeleton during chemotactic stimulation of *Dictyostelium discoideum*. *Cell Motil. Cytoskeleton.* 13:57–63.

Egelhoff, T., and J. Spudich. 1991. Molecular genetics of cell migration: *Dictyostelium* as a model system. *Trend Genet.* 7:161–166.

Fukui, Y., 1993. Towards a new concept of cell motility: Cytoskeletal dynamics in amoeboid movement and cell division. *Int. Rev. Cytol.* 144: 85–127.

Gorlin, J. B., R. Yamin, S. Egan, M. Stewart, T. P. Stossel, D. J. Kwiatkowski, and J. H. Hartwig. 1990. Human endothelial actin-binding protein (ABP-280, nonmuscle filamin): a molecular leaf spring. *J. Cell Biol.* 111:1089–1105.

Hall, A. L., A. Schlein, and J. Condeelis. 1988. Relationship of pseudopod extension to chemotactic hormone-induced actin polymerization in amoeboid cells. *J. Cell. Biochem.* 37:285–299.

Hall, A., V. Warren, S. Dharmawardhane, and J. Condeelis. 1989. Identification of actin nucleation activity and polymerization inhibitor in amoeboid cells: Their regulation by chemotactic stimulation. *J. Cell Biol.* 109:2207–2213.

Hartwig, J. 1992. Mechanisms of actin rearrangements mediating platelet activation. *J. Cell Biol.* 118:1421–1442.

Hartwig, J., and P. Shevlin. 1986. The architecture of actin filaments and the ultrastructural location of actin-binding protein in the periphery of lung macrophages. *J. Cell Biol.* 103:1007–10020.

Hartwig, J. H., and H. L. Yin. 1988. The organization and regulation of the macrophage cytoskeleton. *Cell Motil. Cytoskeleton.* 10:117–125.

Hartwig, J., and D. Kwiatkowski. 1991. Actin binding proteins. *Curr. Opin. Cell Biol.* 3:87–97.

Hell, S., G. Reiner, C. Cremer, E. H. K. Stelzer. 1993. Aberrations in confocal fluorescence microscopy induced by mismatches in refractive index. *J. Microsc. (Oxford)* 169:391–405.

Hock, R. S., and J. S. Condeelis. 1987. Isolation of a 240-kilodalton actin-binding protein from *Dictystelium discoideum*. *J. Biol. Chem.* 262:394–400.

Lee, J., A. Ishihara, J. A. Theriot, and K. Jacobson. 1993. Principles of locomotion for simple-shaped cells. *Nature (Lond.).* 362:167–171.

Lewis, A., and P. Bridgeman. 1992. Nerve growth cone lamellipodia contain two populations of actin filaments that differ in organization and polarity. *J. Cell Biol.* 119:1219–1243.

Luna, E., and A. Hitt. 1992.Cytoskeleton-plasma membrane interactions. *Science (Wash. DC).* 258:955–964.

Niederman, R., P. C. Amrein, and J. Hartwig. 1983. Three- dimensional structure of actin filaments and of an actin gel made with actin-binding protein. *J. Cell Biol.* 96:1400–1413.

Noegel, A. A., S. Rapp, F. Lottspeich, M. Schleicher, and M. Stewart. 1989. The *Dictyostelium* gelation factor shares a putative actin binding site with α-actinins and dystrophin and also has a rod domain containing six 100-residue motifs that appear to have a cross-beta conformation. *J. Cell Biol.* 109:607–618.

Ogihara, S., J. Carboni, and J. Condeelis. 1988. Electron microscopic localization of myosin II and ABP-120 in the cortical matrix of *Dictyostelium* amoebae using IgG-gold conjugates. *Dev. Genet.* 9:505–520.

Ohta, Y., T. Stossel, and J. Hartwig. 1991. Ligand-sensitive binding of actin-binding protein to immunoglobulin G Fc receptor (FcγRI). *Cell.* 67:275–282.

Omann, G., R. Allen, G. Bokoch, R. Painter, A. Traynor, and L. Sklar. 1987. Signal transduction and cytoskeletal activation in the neutrophil. *Physiol. Rev.* 67:285–322.

Oster, G. 1984. On the crawling of cells. *J. Embryol. Exp. Morph.* 83:329–364.

Oster, G., and A. Perelson. 1995. Cell protrusions. *In* Lecture Notes In Biomathematics. Vol. 100. S. Levin, editor. Springer Verlag, New York. In press.

Podolski, J., and T. Steck. 1990. Length distribution of F-actin in *Dictyostelium discoideum*. *J. Biol. Chem.* 265:1312–1318.

Titus, M. A., D. Wessels, J. A. Spudich, and D. Soll. 1993. The unconventional myosin encoded by the myoA gene plays a role in *Dictyostelium* motility. *Mol. Biol. Cell.* 4:233–246.

Visser, T. D., J. L. Oud, and G. J. Brakenhoff. 1992. Refractive index and axial distance measurements in 3-D microscopy. *Optik.* 90:17–18.

Wells, K. S., D. R. Sandison, J. Strickler, and W. W. Webb. 1990. Quantitative fluorescence imaging with laser scanning confocal microscopy. *In* Handbook of Biological Confocal Microscopy. J. B. Pawley, editor. Plenum Press, New York. 27–39.

Wessels, D., D. R. Soll, D. Knecht, W. F. Loomis, A. DeLozanne, and J. Spudich. 1988. Cell motility and chemotaxis in amebae lacking myosin heavy chain. *Dev. Biol.* 128:164–177.

Wessels, D., J. Murray, G. Jung, J. A. Hammer III, and D. R. Soll. 1991. Myosin IB null mutants of *Dictyostelium* exhibit abnormalities in motility. *Cell Motil. Cytoskeleton.* 20:301–315.

Wilson, T. 1990. The role of the pinhole in confocal imaging systems. *In* Handbook of Biological Confocal Microscopy. J. B. Pawley, editor. Plenum Press, New York. 113–126.

Wolosewick, J. J., and J. Condeelis. 1986. Fine structure of gels prepared from an actin-binding protein and actin: comparison to cytoplasmic extracts and cortical cytoplasm in amoeboid cells of *Dictyostelium discoideum*. *J. Cell Biochem.* 30:227–243.

Zigmond, S. H. 1993. Recent quantitative studies of actin filament turnover during cell locomotion. *Cell Motil. Cytoskeleton.* 25:309–316.